Implications of Surface Charge and Curvature for the Binding Orientation of *Thermomyces lanuginosus* Lipase on Negatively Charged or Zwitterionic Phospholipid Vesicles As Studied by ESR Spectroscopy†

Eva M. K. Hedin,‡ Pernille Høyrup,§ Shamkant A. Patkar,|| Jesper Vind,|| Allan Svendsen,|| and Karl Hult*,‡

School of Biotechnology, Department of Biochemistry, Royal Institute of Technology, AlbaNova University Center, SE-106 91 Stockholm, Sweden, Department of Chemistry, Building 207, Technical University of Denmark, DK-2800 Kgs. Lyngby, Denmark, and Novozymes A/S, Smørmosevej 25, DK-2880 Bagsvaerd, Denmark

Received July 26, 2005; Revised Manuscript Received October 6, 2005

ABSTRACT: The triglyceride lipase (EC 3.1.1.3) *Thermomyces lanuginosus* lipase (TLL) binds with high affinity to unilamellar phospholipid vesicles that serve as a diluent interface for both lipase and substrate, but it displays interfacial activation on only small and negatively charged such vesicles [Cajal, Y., et al. (2000) *Biochemistry 39*, 413−423]. The productive-mode binding orientation of TLL at the lipid−water interface of small unilamellar vesicles (SUV) consisting of 1-palmitoyl-2-oleoyl-*sn*-glycero-3-phosphatidylglycerol (POPG) was previously determined using electron spin resonance (ESR) spectroscopy in combination with site-directed spin-labeling [Hedin, E. M. K., et al. (2002) *Biochemistry 41*, 14185−14196]. In our investigation, we have studied the interfacial orientation of TLL when bound to large unilamellar vesicles (LUV) consisting of POPG, and bound to SUV consisting of 1-palmitoyl-2-oleoyl-*sn*-glycero-3-phosphatidylcholine (POPC). Eleven single-cysteine TLL mutants were spin-labeled as previously described, and studied upon membrane binding using the water soluble spin-relaxation agent chromium(III) oxalate (Crox). Furthermore, dansyl-labeled vesicles revealed the intermolecular fluorescence quenching efficiency between each spin-label positioned on TLL, and the lipid membrane. ESR exposure and fluorescence quenching data show that TLL associates closer to the negatively charged PG surface than the zwitterionic PC surface, and binds to both POPG LUV and POPC SUV predominantly through the concave backside of TLL opposite the active site, as revealed by the contact residues K74C-SL, R209C-SL, and T192C-SL. This orientation is significantly different compared to that on the POPG SUV, and might explain the differences in activation of the lipase. Evidently, both the charge and accessibility (curvature) of the vesicle surface determine the TLL orientation at the phospholipid interface.

Triglyceride lipases (EC 3.1.1.3, triacylglycerol lipase) are enzymes that hydrolyze long-chain triglycerides at a lipid−water interface. Lipases are ubiquitous in nature, and have been isolated from many sources, including animals (*1*), plants (*2*), bacteria (*3*), moulds (*4*), and fungi (*5*). The hydrolysis products of lipase action (di- and monoglycerides, glycerol, and free fatty acids) are readily taken up by an organism, whereas triglycerides are unable to pass cellular membranes (*6*), and the intestinal barrier in higher animals (*7*). Thus, lipases are essential for the metabolization of fats in living organisms, and are also responsible for the circulation (flow) in nature of the large biomass that lipids comprise (*7*). Lipases have many interesting industrial applications (*8*), and are furthermore often highly active on unnatural substrates, such as monoesters, displaying pronounced regio- and stereoselectivities. Consequently, lipases are useful as catalysts in organic chemistry for the biotransformation of biologically active compounds or building blocks (*9*).

Lipases belong to the α/β hydrolase group (*10*), sharing several traits of this family, such as the α/β hydrolase fold (*11*), and an active-site catalytic triad consisting of Ser, His, and Asp/Glu, despite a relatively high degree of diversity in the amino acid sequences of lipases. Indeed, lipases have long been viewed as a special group of esterases that have the additional ability to hydrolyze the ester bond of long-chain fatty acid glycerol esters. Unlike esterases, however, lipases display low activity on monomeric substrates in aqueous solution, but become highly activated when substrates aggregate near their critical micellar concentration (cmc).[1] This dependence of an interface for full activity was termed in 1958 by Sarda and Desnuelle "interfacial activation" (*12*). Other interfaces, such as glass walls or gas bubbles (*13*, *14*), are also known to induce this activation, as well as certain detergents and organic solvents (*15*−*17*).

Several X-ray structures of lipases have been determined at high resolution (*1*, *18*−*22*) in closed or open conformations, with bound inhibitors or cocrystallized with micelles

† This work was supported by the European Commission (Contract BIO4-CT972365).

* To whom correspondence should be addressed. Phone: +46 8 5537 8364. Fax: +46 8 5537 8468. E-mail: kalle@biotech.kth.se.

‡ Royal Institute of Technology.

§ Technical University of Denmark.

|| Novozymes A/S.

10.1021/bi051478o CCC: $30.25
Published on Web 11/24/2005

(*23*−*27*). In addition to showing the typical fold and the active-site residues, the structures have revealed that most (but not all) lipases have a "lid", i.e., a short α-helix covering the active-site cavity of lipases in the closed conformation (*10*). The lid can rotate open around its hinges, granting access of the active site to the substrate, at the same time that a large hydrophobic patch is formed, facilitating adsorption to the lipid interface (*28*, *29*). It is believed that the open and closed lipase conformations, reflected in the X-ray structures, exist in equilibrium in aqueous solution [mostly shifted toward the closed state (*30*)] and that they represent the start and end structures in the interfacial activation pathway (*29*, *31*). The mechanism of interfacial activation or its discrete intermediate steps are not fully elucidated at present. However, evidence for some intermediate, activated forms of lipase has recently been reported through new X-ray structures (*32*), and through conformers "trapped" in solution using rapid freeze-drying (*33*).

Although the X-ray structures provide important structural data of lipases, the protein crystals are grown under extreme conditions and provide only static information. However, using spectroscopic methods, enzyme dynamics and interactions can be studied under conditions that are physiologically relevant. The lipase from the filamentous fungus *Thermomyces lanuginosus*, TLL, is one of the well-studied lipases, and displays classical interfacial activation (*34*). TLL has been cloned and overexpressed (*35*, *36*), and several TLL X-ray structures have been determined (*22*, *26*, *32*). TLL is a glycosylated, 33 kDa, 269-amino acid enzyme that has a pH optimum of 11−12 (*37*), and displays maximal in vitro activity for triglycerides with a chain length of 12 carbons (*32*). Since triglycerides are not amphiphilic molecules, and are poorly soluble in water, they do not form well-defined aggregates of known morphology and surface area (*13*). This is a severe complication in studying the kinetics and dynamics of triglyceride lipases. However, Berg et al. (*13*) developed a system in which unilamellar vesicles, consisting of phospholipids, served as a diluent interface of well-defined composition, to which both the lipase and various (codispersed) substrates could bind and then react. Phospholipids themselves are not substrates of lipases, since the phospholipid molecule has a poor affinity for the active site, due to its negative charge (*13*). Using fluorescence spectroscopy, Berg et al. and Cajal et al. showed that TLL binds to vesicles consisting of 1-palmitoyl-2-oleoyl-*sn*-glycero-3-phosphatidylglycerol (POPG) or 1-palmitoyl-2-oleoyl-*sn*-glycero-3-phosphatidylcholine (POPC) with similar high affinity (*13*, *38*). Furthermore, TLL was shown to display interfacial activation on small unilamellar vesicles (SUV) of POPG, with a 100-fold increase in activity for substrates partitioned at the vesicle interface, compared to the activity with the monomeric substrates. Interestingly, this activation was not seen on large unilamellar (LUV) POPG, or on the zwitterionic vesicles, independent of vesicle size (*13*, *38*).

Electron spin resonance (ESR) spectroscopy combined with site-directed spin-labeling (SDSL) of proteins has proven to be a powerful technique for studying protein interactions and dynamics (*39*). Our group has previously presented several single-cysteine mutants of TLL, for which we employed SDSL to introduce a spin-label at specific sites in the protein (*40*). We used ESR spectroscopy in conjunction with spin-relaxation agents and electrostatic-potential-based modeling (*41*) to study the orientation of the productive mode of TLL bound to the POPG SUV. This afforded the first experimental evidence of the detailed molecular orientation at the lipid−water interface for a triglyceride lipase (*40*).

In this paper, we have studied the orientation of TLL when bound to the negatively charged, large unilamellar vesicles consisting of POPG, or to the zwitterionic, small unilamellar vesicles consisting of POPC. The aim was to elucidate how these binding orientations differ from the active-mode binding orientation previously found for TLL on the POPG SUV (*40*). We also wanted to discover the way in which the vesicle phospholipid composition dictates the binding orientation of TLL, and how this is related to the observed variations in lipase activation. As in our preceding study, 11 single-cysteine mutants with the mutations scattered around the surface of TLL have been spin-labeled with a nitroxide spin-label (SL), and studied by ESR spectroscopy (*40*). The accessibility of each spin-label to the aqueous surroundings was mapped for the membrane-bound SL-TLLs, utilizing the water-soluble spin-relaxation agent chromium(III) oxalate, Crox (*42*). In addition, the interaction of each spin-label with the lipid membrane was assessed by nitroxide quenching of fluorescence, for the SL-TLLs bound to dansyl-labeled vesicles. The data revealed that the binding orientation of TLL differs significantly between the vesicles having different surface charge or membrane curvature, despite the fact that TLL binds to these vesicles with similar dissociation constants, K_d (*38*). Spectral data are compared for the three vesicle systems, and the prerequisite driving forces for the interfacial activation of TLL on the diluent phospholipid interfaces are discussed.

EXPERIMENTAL PROCEDURES

General. The spin-labeling reagent (1-oxyl-2,2,5,5-tetramethyl-Δ^3-pyrroline-3-methyl) methanethiosulfonate (MTSL) was from Toronto Research Chemicals Inc. (Toronto, ON). The lipid fluorophore *N*-[5-(dimethylamino)naphthalene-1-sulfonyl]-1,2-dihexadecanoyl-*sn*-glycero-3-phosphatidylethanolamine triethylammonium salt (dansyl-DHPE) and the C16 alkyl-chain quartenary amine spin-label, 4-(*N*,*N*-dimethyl-*N*-hexadecyl)ammonium-2,2,6,6-tetramethylpiperidine-1-oxyl-iodide (CAT 16), were from Molecular Probes Europe BV (Leiden, The Netherlands). The phospholipids 1-palmitoyl-2-oleoyl-*sn*-glycero-3-phosphatidylglycerol (POPG) and 1-palmitoyl-2-oleoyl-*sn*-glycero-3-phosphatidylcholine (POPC)

[1] Abbreviations: CAT 16, 4-(*N*,*N*-dimethyl-*N*-hexadecyl)ammonium-2,2,6,6-tetramethylpiperidine-1-oxyl-iodide; cmc, critical micellar concentration; Crox, chromium(III) oxalate; CW, continuous wave; dansyl-DHPE, *N*-[5-(dimethylamino)naphthalene-1-sulfonyl]-1,2-dihexadecanoyl-*sn*-glycero-3-phosphatidylethanolamine triethylammonium salt; DTT, DL-dithiothreitol; EDTA, ethylenediaminetetraacetic acid; ESR, electron spin resonance; GA, gum arabicum; HEPES, *N*-(2-hydroxyethyl)-piperazine-*N*′-2-ethanesulfonic acid; K_{SV}, Stern−Volmer quenching constant; LU, lipase unit; LUV, large unilamellar vesicles; MLV, multilamellar vesicles; MS, mass spectrometry; MTSL, 1-oxyl-2,2,5,5-tetramethyl-Δ^3-pyrroline-3-methyl methanethiosulfonate; POPC, 1-palmitoyl-2-oleoyl-*sn*-glycero-3-phosphatidylcholine; POPG, 1-palmitoyl-2-oleoyl-*sn*-glycero-3-phosphatidylglycerol; SDS−PAGE, sodium dodecyl sulfate−polyacrylamide gel electrophoresis; SDSL, site-directed spin-labeling; SL, spin-labeled; SUV, small unilamellar vesicles; Tris, tris-(hydroxymethyl)aminomethane; TLL, *T. lanuginosus* lipase; SL-TLL (and TLL-SL), spin-labeled *T. lanuginosus* lipase.

were from Avanti Polar Lipids (Birmingham, AL). The spin-relaxation agent chromium(III) oxalate (Crox) was synthesized by the method of Bailar and Jones (*43*). PD-10 desalting columns were from Amersham Pharmacia Biotech (Uppsala, Sweden), and Slide-A-Lyzer dialysis cassettes (10 kDa molecular mass cutoff) were from Pierce (Boule Nordic AB, Huddinge, Sweden). Ultrapure water (resistivity $\rho \geq 18.2$ MΩ cm^{-1}) was used in all analyses, and all bulk chemicals were analytical grade or better.

Production of Lipase Variants. The gene encoding the lipase from *T. lanuginosus* was cloned, sequenced, transformed into *Aspergillus oryzae*, expressed, and purified as described elsewhere (*35*, *36*, *44*). We employed the same lipase variants as in our previous study, with the single-cysteine mutations scattered around the surface of TLL (*40*). Thus, substitution of a chosen surface residue with cysteine yielded the following variants: P42C (proline 42 exchanged for cysteine), G61C, K74C, D96C, T123C, D137C, T192C, R209C, T231C, I252C, and T267C. The presence of the correct cysteine mutation in each variant was verified by gene sequencing. Required purity, folding, and lipolytic activity of the produced recombinant proteins were confirmed by SDS−PAGE, electrospray MS, fluorescence spectroscopy, and pH-stat activity measurements.

Site-Directed Spin-Labeling of TLL Single-Cysteine Mutants. The spin-labeling procedure for the TLL single-cysteine mutants has been described in detail previously (*44*). Briefly, each recombinant protein was gently reduced [1 mg/mL protein in 50 mM Tris-acetate and 2 mM EDTA (pH 7.7)] with 0.3 mM DTT (from a freshly prepared stock solution) for 1 h at room temperature. The DTT was removed by dialysis, and then 45 molar equiv of the spin-labeling reagent MTSL was immediately added to the stirred protein solution from a freshly prepared stock solution in ethanol [final content of ethanol of 1.5% (v/v)]. After 1 h, the reaction mixture was purified by gel filtration on a PD-10 column pre-equilibrated with 20 mM sodium-HEPES (pH 7.0) followed by extensive dialysis against the same buffer at 4 °C. Wild-type TLL was used as a control in all reactions, confirming that there was no unspecific insertion of spin-label in the enzyme. The spin concentration of the spin-labeled TLL mutants was determined by continuous wave (CW) ESR spectroscopy against MTSL standard solutions, and the protein concentration was determined from the absorbance at 280 nm using an extinction coefficient of 35 920 cm^{-1} M^{-1} based on amino acid composition (*45*). The degree of spin-label incorporation was found to range between 0.1 and 1.0 (moles of spin-label per mole of protein) for the different mutants. Lipase-specific hydrolytic activity was assayed on an emulsion of glyceryl tributanoate (tributyrin) and gum arabicum (GA), using the pH-stat method as described elsewhere (*35*). One lipase unit (LU) is defined as 1 μmol of released titratable acid per minute. The spin-labeled enzymes were stored as aliquots at −20 °C and were stable for several months.

Preparation of Unilamellar Phospholipid Vesicles. Unilamellar phospholipid vesicles consisting of either POPG or POPC prepared to a diameter of 50 nm (SUV) and 100 nm (LUV), and labeled vesicles with POPG or POPC, containing the lipid fluorophore dansyl-DPHE, or the lipid spin-label CAT 16 (99:1 lipid:label molar ratio), were all prepared by the following procedure. Weighed amounts of the appropriate lipids were dissolved in a 1:1 (v/v) chloroform/methanol mixture. The organic solvent was evaporated under a weak stream of nitrogen, and the samples were kept under vacuum overnight. Buffer [20 mM sodium-HEPES (pH 7.0)] was added to the dried lipid film for hydration, forming multilamellar vesicles (MLV) at 55 °C for at least 30 min with extensive vortexing every 10 min. SUV were formed by extrusion twice through two stacked 100 nm size polycarbonate filters and 10 times through two stacked 50 nm size polycarbonate filters. LUV were prepared by extrusion twice through two 200 nm filters and 10 times through two 100 nm filters, with all filters stacked. The size distribution of the vesicles was analyzed by dynamic light scattering, using a Malvern Zetasizer (Malvern Instruments Ltd., Malvern, U.K.).

Fluorescence Quenching Experiments. Intermolecular quenching of the fluorescence from dansyl-labeled phospholipid vesicles by the spin-labeled TLL mutants (*46*) was monitored in 20 mM sodium-HEPES buffer at pH 7.0 and 25 °C. The unlabeled (reference) or spin-labeled TLL mutant (the quencher) was titrated to a 1 mM suspension of small lipid vesicles (SUV) consisting of POPC and dansyl-DHPE in a 99:1 molar ratio, or to a 1 mM suspension of large lipid vesicles (LUV) consisting of POPG and dansyl-DHPE in a 99:1 molar ratio. The fluorescence was monitored at 500 nm with the excitation set at 350 nm, using a SLM DMX-1100 spectrofluorimeter (SLM Instruments Inc., Urbana, IL). The final concentration of protein was less than 10 μM. The fluorescence data were analyzed according to the Stern−Volmer equation for collisional quenching:

$$F_0/F = 1 + K_{SV}[Q] \quad (1)$$

where F_0 and F are the intensities of fluorescence in the absence and presence of quencher, respectively, K_{SV} is the Stern−Volmer quenching constant, and [Q] is the molar concentration of quencher.

ESR Spectroscopy. CW ESR spectra were recorded on a Bruker (Rheinstetten, Germany) EMX ESR spectrometer with a 12 kW 10″ magnet in the X-band at 9.75 GHz, using a Bruker ER 4102 ST standard resonator. The conversion efficiency factor of the resonator, α, was estimated to be 1 $G/W^{1/2}$. Spectra were recorded at room temperature with a receiver gain of 4.48×10^4 unless stated otherwise, and 1 G, 100 kHz magnetic field modulation for phase-sensitive detection. A field modulation of 1 G ensures a well-defined signal, and the line broadening due to overmodulation is less than 10% (*47*). All measurements were performed at subsaturating microwave amplitudes ($h_1 < 0.36$ G), under critical coupling conditions, and the spectra were recorded several times and summed to improve the signal-to-noise ratio. All samples (50 μL) were prepared in 20 mM sodium-HEPES buffer (pH 7.0) and loaded into 1 mm (inside diameter) quartz tubes sealed at one end. Reproducible positioning of the quartz tubes in the resonator was ensured by use of a Teflon stopper. Spectra of spin-labeled phospholipid vesicles were recorded at 100 mW for CAT 16 incorporated in small and large POPG vesicles, as well as small and large POPC vesicles. Crox was added to a 10 mM lipid suspension from a 0.5 M stock solution, for a final Crox concentration of 0−9.8 mM. Relaxation spectra were recorded for each spin-labeled TLL mutant (15 μM) as a function of incident power

Scheme 1: Representation of the Reaction between MTSL and a Protein Cysteinyl Side Chain

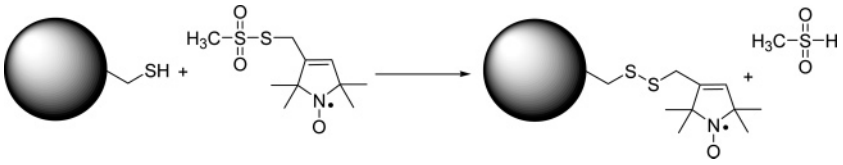

(P_0 < 127 mW). First, spectra were recorded in the absence and presence of phospholipid vesicles (3 mM POPG LUV or POPC SUV). Subsequently, Crox was added from the stock solution for a final concentration of 9.8 mM, and the samples were analyzed again. The spectral intensity of the Crox-containing samples was corrected for dilution effects.

ESR Theory and Data Analysis. The peak-to-peak line width of the central resonance line in the ESR spectra, δ, was used to determine the semiquantitative parameter entitled scaled mobility, M_s (*39*), for each protein-bound nitroxide according to the relation $M_s = (\delta^{-1} - \delta_i^{-1})/(\delta_m^{-1} - \delta_i^{-1})$. The parameters δ_m and δ_i represent the line widths of the most and least mobile nitroxide spin-labels, respectively, observed for a model system based on rhodopsin. The established values for δ_m and δ_i of 2.1 and 8.4 G, respectively, were used. ESR relaxation spectroscopy using Crox was performed with the low microwave-amplitude method (*48*), which employs only low and subsaturating microwave amplitudes (h_1 < 0.36 G). The theoretical basis and experimental considerations of this method have been discussed in depth previously (*48*). In brief, at subsaturating microwave amplitudes, the peak-to-peak height of the central resonance line in the first-derivative ESR spectrum, ΔY, is given by (*41*, *48*, *49*)

$$\Delta Y \approx cP_0^{1/2} = c'T_{2e}^{2}P_0^{1/2} \qquad (2)$$

where c is an (adjustable) composite gain constant, T_{2e} is the spin−spin relaxation time, and P_0 is the microwave incident power. The constant c' is defined as $0.7q\gamma_e h_m\alpha$, where $q = \hbar/(NkT)$, γ_e is the electron gyromagnetic ratio, and h_m is the Zeeman modulation field amplitude (*48*, *49*). The microwave amplitude (in gauss), h_1, acting on the sample is dependent on the conversion efficiency factor of the resonator, α, according to the relation $h_1 = \alpha P_0^{1/2}$. The spin−spin relaxation rate, R_2, is related to the spin−spin relaxation time through the relation $R_2 = (\gamma_e T_{2e})^{-1}$ (*41*, *49*). Hence, the linear dependence of ΔY on the square root of the incident power (at low microwave amplitudes) is given by the proportionality constant, c, as $c = c'(R_2\gamma_e)^{-2}$, which means that $c^{-1/2}$ is directly proportional to the spin−spin relaxation rate, R_2 (*48*). The presence of a spin-relaxation agent, e.g., Crox, changes the relaxation rates of a spin-label in a concentration-dependent manner through Heisenberg exchange (*50*, *51*). Accordingly, with the addition of Crox, the change in $c^{-1/2}$ is proportional to the local Crox concentration (*41*, *48*):

$$\Delta c^{-1/2} = \gamma_e c'^{-1/2}\chi[\text{Crox}] \qquad (3)$$

where χ is the relaxivity of the spin-label. The exposure factor, Φ, is defined as a measure of the exposure to the aqueous surroundings (and a water-soluble spin-relaxation agent) for a spin-label on the surface of a protein adsorbed to a lipid membrane, and is given by (*41*, *48*)

$$\Phi = \frac{(\Delta c^{-1/2})_{+\text{membrane}}}{(\Delta c^{-1/2})_{-\text{membrane}}} = \frac{[\text{Crox}]^{\text{local}}_{+\text{membrane}}}{[\text{Crox}]^{\text{local}}_{-\text{membrane}}} \qquad (4)$$

Spectral relaxation data were analyzed as follows. Proportionality constants, c, were attained by a linear regression analysis of the central resonance amplitudes obtained as a function of incident power, using at least four data points for each data set. Low-amplitude parameters, $\Delta c^{-1/2}$, were obtained as the difference in the inverse square root of c upon addition of Crox. Finally, exposure factors were calculated using the $\Delta c^{-1/2}$ obtained in the presence or absence of lipid vesicles (*48*).

RESULTS

Characteristics of Spin-Labeled Lipase Mutants. Proteins can be routinely spin-labeled at most desired positions in the amino acid sequence by the approach of site-directed spin-labeling (*52*). This involves introducing a cysteine into the protein by site-directed mutagenesis and concomitant spin-labeling with a sulfhydryl-specific reagent, such as MTSL (Scheme 1). In our study, we used the same 11 single-cysteine mutants of TLL presented previously (*40*), for comparative purposes also. The single-cysteine mutations are strategically placed to provide a near coverage of the protein surface, as shown in Figure 1. Five of the single-cysteine substitution mutations (T267C, I252C, R209C, D96C, and G61C) are positioned surrounding the active-site region on the top half of the protein. On the lower half, P42C, T231C, T192C, and T123C form a ring around the enzyme, and K74C and D137C are placed right at the bottom of the central β-sheet core. Although all these positions are superficial in the protein, they provide different topographies at the point of attachment of the spin-label. Residues P42C, T123C, and R209C are located in α-helices. T192C is on a β-sheet. G61C, K74C, D137C, and T231C reside in β-turns or β-hairpins. D96C, I252C, and T267C are positioned in loops (additionally, P42C and T267C are close to two different disulfide bridges).

As reported previously, spin-labeling of the TLL mutants with MTSL afforded correctly folded and highly functional proteins in all cases (*40*). The lipolytic activity of the cysteine mutants was comparable to that of the wild-type lipase (5700 LU/mg), before as well as after spin-labeling, with mutant specific activities ranging between 3500 and 6500 LU/mg when assayed by the pH-stat method on an emulsion of tributyrin. This is consistent with the observation that the nitroxide generally does not perturb protein structure, enzymatic activity, or thermal stability, with the weakest effects expected for solvent-exposed labeling sites (*53*). The spin-labeling was confirmed to be specific to the cysteine side chain, and resulted in quantitative labeling or less, which

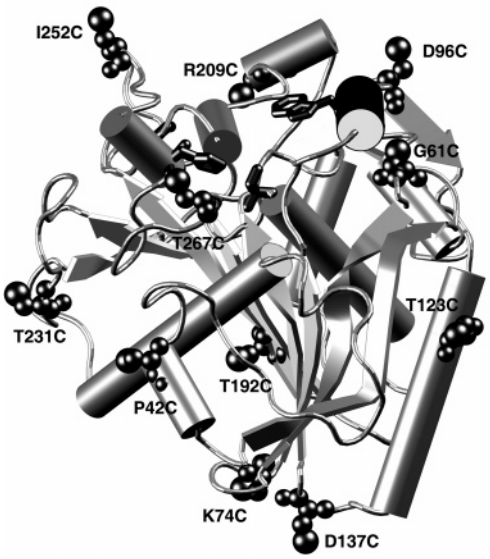

FIGURE 1: Structure of *T. lanuginosus* lipase (TLL) in the open conformation showing the position of each single-cysteine mutation (black space-filling portion) and displaying the characteristic α/β-hydrolase fold of lipases. The active-site catalytic triad, consisting of Ser146, His258, and Asp201, is highlighted (black tube) together with the lid region containing the classical Trp89 in the lid. The complexed *n*-dodecyl phosphonate inhibitor was omitted for clarity [the TLL atomic coordinates were provided by Lawson and Brzozowski (*26*)]. This cartoon representation was generated with POV-Ray and VMD (*73*).

was found to correlate with the accessibility of the attachment site in the various recombinant proteins (*40*). The ESR spectra of the spin-labeled TLL mutants have been presented previously (*40*). The spectra are representative of a nitroxide spin-label with rapid, nearly isotropic rotation, which is consistent with nitroxides attached to superficial sites in a protein. Rotational correlation times, τ_c, are quantitatively found to be in the range of 1 ns, characteristic of nitroxides situated on α-helices or surface loops (*39*).

Large and small unilamellar phospholipid vesicles consisting of POPG and POPC, respectively, were prepared, inspected by dynamic light scattering, and found to have a diameter of 84.5 with a polydispersity of 0.156 (POPG LUV) and a diameter of 67.4 nm with a polydispersity of 0.075 (POPC SUV), respectively. Next, the spin-label dynamics of each spin-labeled TLL mutant were studied by ESR spectroscopy upon binding to the negatively charged POPG vesicles, or to the zwitterionic POPC vesicles. The scaled mobility, M_s, is a semiquantitative measure of spin-label mobility, determined from the peak-to-peak line width, δ, of the central resonance line in the first-derivative ESR spectrum (*39*). In principle, both the rate and the amplitude of the nitroxide motion are manifested in the value of M_s, and M_s has been shown to correlate well with τ_c for motions on helices (*54*). In Figure 2, values of M_s are shown for the spin-labeled TLL mutants in aqueous solution (dark gray bars) and adsorbed to vesicles (light gray bars) consisting of POPC SUV, POPG LUV, or POPG SUV (the latter values taken from ref *40*). Values of 0 and 1 correspond to the least and most mobile ESR line shapes, respectively, obtained from the nitroxide side chain in proteins, based on a model system with rhodopsin (*54*). As seen in Figure 2, the spin-labeled TLL mutants have values of M_s ranging from approximately 0.8 to 1.4, which means that these are among

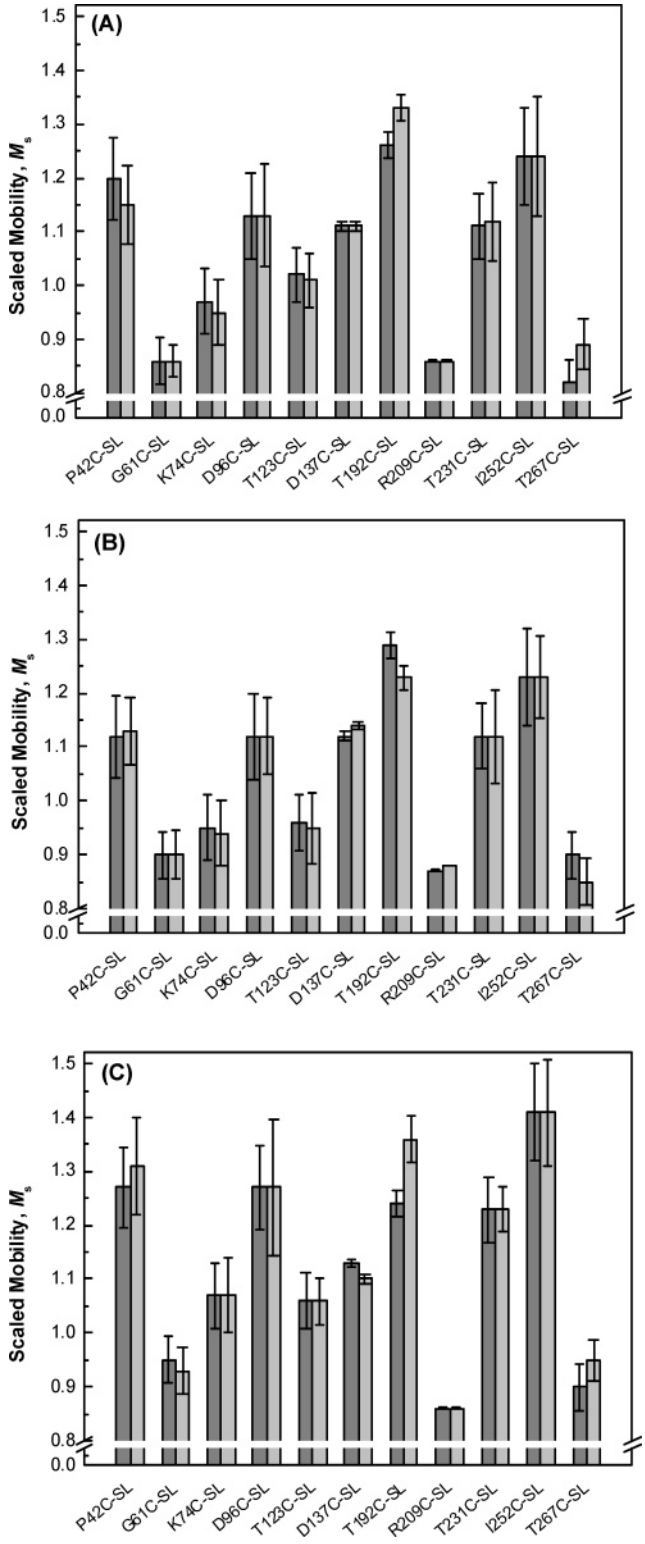

FIGURE 2: Scaled mobility, M_s, of spin-labeled TLL mutants in solution (dark gray bars) or bound to the unilamellar phospholipid vesicles (light gray bars): POPC SUV (A), POPG LUV (B), and POPG SUV (C). Values for POPG SUV were taken from ref *40*. Errors in M_s were determined as the error propagation of the ESR line width standard deviation of triplicate measurements.

the most mobile nitroxides seen in proteins. That some of the values exceed 1 is not surprising, since the reference system is based on spin-labels positioned on a transmembrane protein, whereas TLL is an excreted peripheral protein. The least mobile nitroxides in TLL are seen for mutants G61C-

Chart 1: Molecular Structure of (A) the Lipid Fluorophore Dansyl-DHPE and (B) the Lipid Spin-Label CAT 16

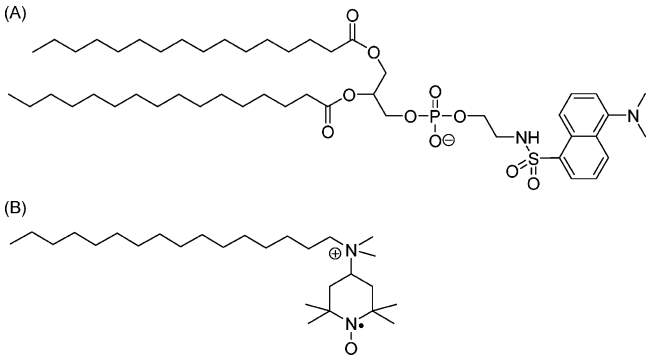

SL, K74C-SL, T123C-SL, R209C-SL, and T267C-SL. Two of these nitroxides are situated in an α-helix; two are in a *β*-turn/hairpin, and one is next to a half-cystine. The small variations in values of M_s seen for the protein alone fall within the error of the measurement. It is evident that there are no, or only discrete, changes in the mobility of the TLL spin-labels upon membrane binding, for any of the three vesicle types. This is consistent with the previous observation that there is no deep penetration of residues of TLL into the lipid membrane when it is bound to POPG SUV (*40*). In fact, limited contact between lipid and protein surfaces distinguishes several peripheral membrane proteins whose membrane interactions are known, for example, bee venom phospholipase A2 (PLA2) and heterotrimeric G protein (*41*, *55*).

Effect of Crox on Spin-Labeled Phospholipid Vesicles. Unilamellar phospholipid vesicles consisting of POPC or POPG were both prepared as SUV and LUV with 1 mol % of the lipid spin-label CAT 16 (Chart 1B) included in the vesicles. ESR relaxation spectroscopy when studying spin-labeled proteins bound to lipid vesicles is founded on nitroxide interactions with spin-relaxation agents, and in this study, we used a strictly water soluble spin-relaxation agent, e.g., Crox. The basis for understanding the relaxation data is that Crox diffuses closely enough to a lipid membrane to interact with a spin-label on the protein bound to the lipid vesicles. Near the negatively charged surface of POPG vesicles, there exists a concentration gradient of Crox compared to its bulk concentration, generated by electrostatic repulsion between the lipid surface and the negatively charged Crox molecule (*41*). For the zwitterionic surface of POPC, however, mainly steric factors will prevail, and the Crox gradient beginning at the lipid surface can thus be expected to be steeper. For that reason, the influence of Crox was investigated for the CAT 16 spin-label, situated at the headgroup level in the prepared phospholipid vesicles with different surface charges and sizes. Crox induces broadening of the ESR spectral peak width, while the peak amplitude decreases (*42*). CW ESR spectra were recorded for the various spin-labeled vesicles together with Crox at concentrations between 0 and 9.8 mM. Figure 3 shows the first-derivative ESR spectra of CAT 16 in the phospholipid vesicles, recorded at 100 mW together with 4.95 mM Crox. The resulting effects of Crox on the spin-labeled vesicles are summarized in Figure 4, in which the central resonance peak-to-peak height, ΔY, and the central resonance line width, δ, in the first-derivative ESR spectra are shown as a

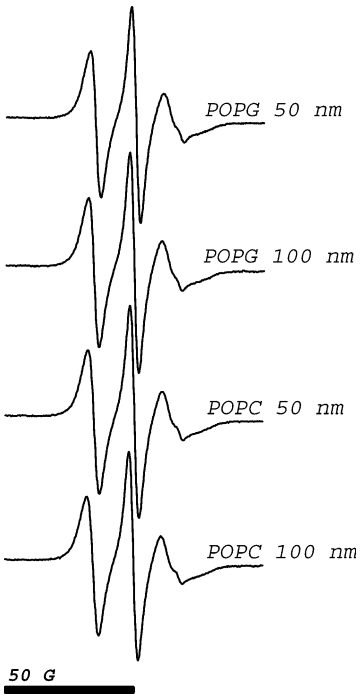

FIGURE 3: First-derivative CW ESR spectra recorded in the X-band at 9.75 GHz of the lipid spin-label CAT 16 incorporated in small or large unilamellar vesicles consisting of POPG or POPC, with Crox (final concentration of 4.95 mM) added to the vesicle suspension. The microwave power was 100 mW; the receiver gain was 6.32×10^4, and the scale of the magnetic field is indicated with a bar.

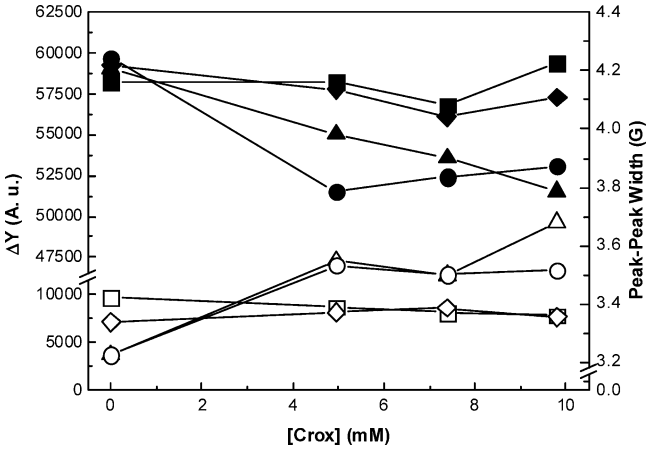

FIGURE 4: Effect of Crox concentration on the ESR central resonance peak-to-peak height, ΔY (black symbols), and the central resonance peak-to-peak width (white symbols) for lipid spin-label CAT 16 (1 mol %) incorporated in the unilamellar vesicles: POPC SUV (triangles), POPC LUV (circles), POPG SUV (squares), and POPG LUV (diamonds).

function of Crox concentration. Several aspects can be inferred from Figure 4. First, the line width (no Crox added) is slightly broader for the POPG vesicles than for the POPC vesicles, which means that for some reason the lipid spin-label is slightly more motionally restricted in the POPG environment. Since lateral diffusion constants of similar lipids do not differ significantly for a lipid PC or PG headgroup (*56*), this small difference in restriction probably has an electrostatic origin. Second, the effect of Crox on both central resonance line width (δ) and peak-to-peak height (ΔY) is more pronounced for the POPC vesicles, with the largest

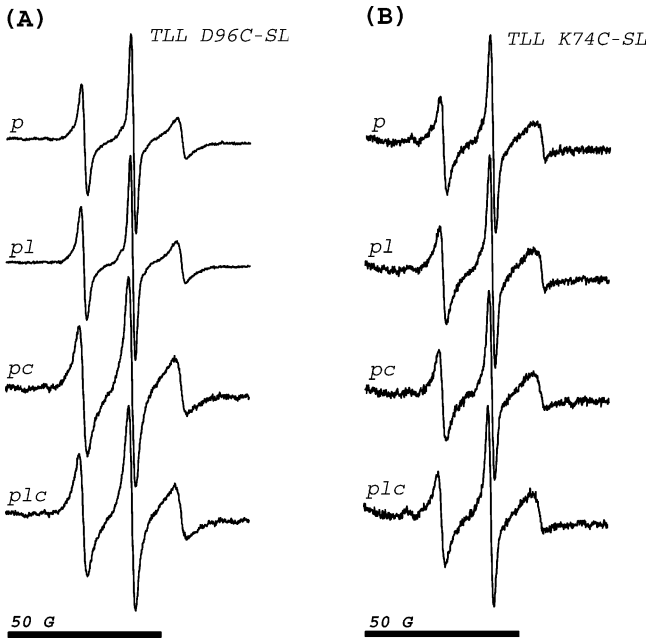

FIGURE 5: First-derivative CW ESR spectra recorded in the X-band at 9.75 GHz of spin-labeled TLL mutants D96C-SL and K74C-SL. Spectra were taken for the protein alone (*p*), the protein bound to lipid vesicles (*pl*), the protein together with 9.8 mM Crox (*pc*), and the protein, lipid, and Crox (*plc*). The lipid was POPG; the scale of the magnetic field is indicated with a bar, and the microwave power was 127 mW.

effect seen with small vesicles. The maximum decrease measured in ΔY was approximately 10−15% for the POPC vesicles, while it was less than 5% for the POPG vesicles. The increase in δ measured was also 10−15% for POPC and a few percent for POPG; however, the line width of the low-field resonance line in the spectra showed almost twice the effect for all vesicles that were studied (data not shown). It can thus be concluded that Crox is close enough to the lipid surfaces to interact with a headgroup label. The observed differences are due to the fact that the local concentration of Crox is higher near the zwitterionic surface of POPC than the negatively charged POPG surface, because of the electrostatic repulsion mentioned earlier. It should be borne in mind, however, that the effects of the spin-relaxation agent here were measured at the level of the phospholipid headgroup within the lipid phase.

Determination of ESR Exposure Factors and Fluorescence Quenching Constants for Spin-Labeled TLL Mutants Bound to POPG and POPC Vesicles. CW ESR spectra were recorded for the spin-labeled TLL mutants as a function of microwave incident power, P_0, in the absence and presence of phospholipid vesicles (lipid:protein molar ratio of 200:1), and in the absence and presence of Crox (9.8 mM). It was confirmed by dynamic light scattering that the addition of lipase or Crox had no effect on the integrity of the vesicles (data not shown). All spectra were recorded at subsaturating microwave amplitudes ($h_1 < 0.36$ G), employing low microwave-amplitude relaximetry (*48*). In Figure 5, first-derivative ESR spectra recorded at 127 mW are shown for a complete experimental set with two of the SL-TLLs. The spin-labeled mutants are representative of an exposed nitroxide (D96C-SL) and a more shielded nitroxide (K74C-SL) upon membrane binding. For each spin-labeled mutant, the low-amplitude proportionality constant, *c*, was determined within each data set, yielding low-amplitude parameters, $\Delta c^{-1/2}$, for the determination of ESR exposure factors, Φ, according to eqs 2−4, respectively. The low-amplitude parameter quantitatively describes Heisenberg exchange between the spin-label and Crox (*48*). The exposure factor is a measure of the degree of exposure to the aqueous phase, for a spin-label on a protein adsorbed to a lipid membrane. The exposure factor is directly proportional to the concentration of Crox in the vicinity of the spin-label and is, furthermore, an indirect measure of the distance from the spin-label to the lipid membrane (*40*, *41*). Φ values of 0 and 1 signify zero exposure and total exposure to Crox, respectively. Values of the exposure factor for the SL-TLLs adsorbed to POPC SUV are listed in Table 1. All values of Φ, ranging between 0.6 and 1.1, are indicative of spin-labels with a medium to high level of exposure to Crox. There are no singular values showing close contact between a spin-label and the membrane. Instead, the values exhibit a flat distribution. This is in sharp contrast to the values obtained earlier with POPG SUV (*40*), and implies that TLL is not that close to the POPC surface. However, assuming that the Crox gradient at the POPC surface is steeper than that for POPG, as indicated by the spin-labeled vesicles, these values would equal lower values of Φ in the POPG system, translating to POPC−membrane distances shorter than the exposure implies. Among the lowest values obtained are those for the spin-labeled mutants K74C-SL, R209C-SL, and T192C-SL. These spin-label positions define a straight vertical line, on the back of TLL in relation to the active-mode contact zone (*40*). This seems to be the side orienting most frequently against the vesicle membrane of POPC SUV.

Table 1: Exposure Factors, Φ, and Stern−Volmer Quenching Constants, K_{SV}, Measured for Spin-Labeled *T. lanuginosus* Lipase Single-Cysteine Mutants Bound to POPC SUV[a]

variant	Φ	K_{SV} (M^{-1})[b]
P42C-SL	1.13 ± 0.38	500 ± 210
G61C-SL	0.82 ± 0.07	1670 ± 360
K74C-SL	0.60 ± 0.18	1780 ± 510
D96C-SL	0.94 ± 0.03	580 ± 100
T123C-SL	0.95 ± 0.21	800 ± 180
D137C-SL	0.89 ± 0.12	390 ± 90
T192C-SL	0.81 ± 0.29	1350 ± 560
R209C-SL	0.65 ± 0.23	1030 ± 220
T231C-SL	0.97 ± 0.03	510 ± 80
I252C-SL	1.13 ± 0.11	120 ± 40
T267C-SL	0.66 ± 0.40	1760 ± 360

[a] Errors given are the calculated error propagations based on the errors from linear fits for *c* or K_{SV}. [b] Measured with dansyl-labeled POPC vesicles (SUV). Values normalized by the degree of spin-label incorporation in the SL-TLL variants.

Fluorescent vesicles were prepared, with 1 mol % of the fluorescence label dansyl-DHPE (Chart 1A) included in the bilayer of POPC SUV and POPG LUV. The fluorescence quenching efficiency was measured for each spin-labeled TLL mutant bound to the labeled vesicles, for which the spin-label acts as a quencher (*46*). The change in fluorescence was first monitored for the vesicles titrated with an unlabeled TLL mutant (reference), and then with a spin-labeled TLL mutant (the quencher) to dissect any contribution of the protein itself from the effect of the nitroxide. Stern−Volmer quenching constants, K_{SV}, were determined as the resulting difference in quenching efficiency, and were normalized by the degree of spin-label incorporation in the proteins. Values

Table 2: Exposure Factors, Φ, and Stern−Volmer Quenching Constants, K_{SV}, Measured for Spin-Labeled *T. lanuginosus* Lipase Single-Cysteine Mutants Bound to POPG LUV[a]

variant	Φ	K_{SV} (M^{-1})[b]
P42C-SL	0.93 ± 0.12	1440 ± 200
G61C-SL	1.36 ± 0.23	1430 ± 230
K74C-SL	0.28 ± 0.18	3260 ± 270
D96C-SL	0.87 ± 0.03	660 ± 70
T123C-SL	0.86 ± 0.22	1430 ± 130
D137C-SL	0.83 ± 0.10	630 ± 90
T192C-SL	0.78 ± 0.25	2970 ± 400
R209C-SL	0.42 ± 0.09	1520 ± 150
T231C-SL	0.88 ± 0.03	880 ± 80
I252C-SL	1.08 ± 0.06	290 ± 40
T267C-SL	0.89 ± 0.34	2750 ± 360

[a] Errors given are the calculated error propagations based on the errors from linear fits for c or K_{SV}. [b] Measured with dansyl-labeled POPG vesicles (LUV). Values normalized by the degree of spin-label incorporation in the SL-TLL variants.

of K_{SV} determined with dansyl-labeled POPC SUV are presented in Table 1, where a high value signifies a high quenching efficiency. It can be seen that the K_{SV} values exhibit a trend similar to that for the exposure factor, with overall low values of quenching efficiency (120−1780 M^{-1}) compared to previous results (*40*), and with an exceptionally flat distribution of the values. In the case of K_{SV}, however, there is no concentration gradient involved. The fluorescence quenching is due to the direct, distance-dependent interaction between the spin-label and the dansyl fluorophore, and dansyl-DHPE is expected to be at a similar position in the lipid headgroup level for all vesicles studied. Therefore, the values of K_{SV} confirm the result obtained with the exposure factor Φ, showing that TLL associates farther from the surface of POPC SUV than that of POPG SUV. This also implies that the concentration gradient of Crox at the zwitterionic POPC interface is not as steep as that assumed in the previous paragraph. The spin-labeled mutants displaying the highest quenching efficiencies were K74C-SL, R209C-SL, and T192C-SL, in agreement with the values of Φ obtained, and also T267C-SL and G61C-SL which are situated on the opposite side of TLL.

Values of the exposure factor for the SL-TLLs bound to POPG LUV are given in Table 2. With these vesicles, there is a wider distribution of Φ values, similar to the situation with POPG SUV seen previously (*40*). Two spin-labeled mutants, K74C-SL and R209C-SL, exhibit quite low levels of exposure to Crox with Φ values of 0.28 and 0.42, respectively. As for the POPC SUV, the region defined by K74C-SL, R209C-SL, and T192C-SL seems to be preferentially oriented toward the membrane surface. Values of K_{SV} obtained with dansyl-labeled POPG LUV are presented in the third column of Table 2. Also the fluorescence quenching efficiency of the SL-TLLs was markedly higher with the POPG LUV, and values were widely distributed, ranging between 290 and 3260 M^{-1}. High quenching efficiency was again seen for the spin-labeled mutants K74C-SL, T192C-SL, R209C-SL, and T267C-SL. Taken together, the ESR and fluorescence data suggest that TLL binds closer to the negatively charged surface of POPG LUV than to the zwitterionic POPC surface. Regardless, TLL seems to bind preferentially with the same orientation on both vesicles, namely, with the backside of the protein facing the lipid membrane.

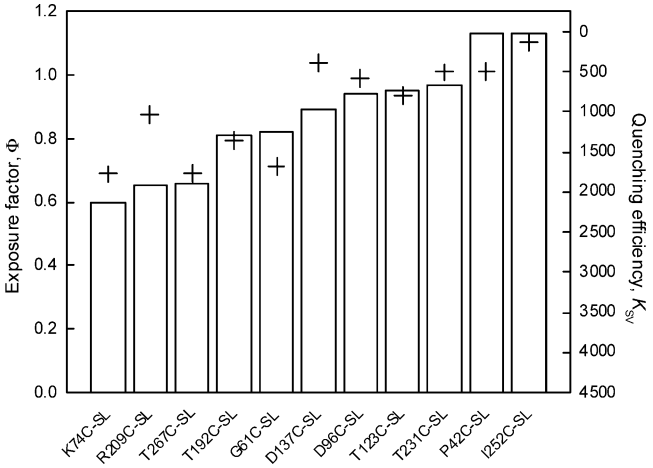

FIGURE 6: Correlation between the ESR exposure factor, Φ (bars), and the fluorescence quenching efficiency constant, K_{SV} (+), for spin-labeled TLL single-cysteine mutants bound to POPC SUV. SL-TLLs are sorted by ascending value of Φ. Error bars were omitted for clarity (errors listed in Table 1).

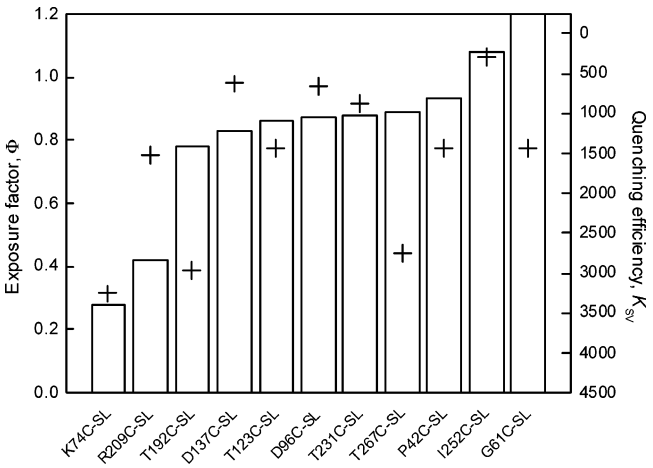

FIGURE 7: Correlation between the ESR exposure factor, Φ (bars), and the fluorescence quenching efficiency constant, K_{SV} (+), for spin-labeled TLL single-cysteine mutants bound to POPG LUV. The value of G61C-SL extends outside the graph and was 1.36 ± 0.23. SL-TLLs are sorted by ascending value of Φ. Error bars were omitted for clarity (errors listed in Table 2).

Comparison of Binding Parameters for TLL on Three Different Phospholipid Vesicles. The ESR exposure factor defines nitroxide interactions with Crox in the aqueous phase, while the fluorescence quenching efficiency quantifies nitroxide−lipid interactions. Thus, these two spectroscopic methods provide complementary information for each spin-label on the surface of TLL when bound at the water−lipid interface. In Figures 6 and 7, the two techniques are compared for TLL bound to POPC SUV and POPG LUV, respectively. For POPC SUV, the values of Φ and K_{SV} are found to correlate well, and the distribution of values is narrow for both parameters. Here, high values of the exposure factor and low values of quenching efficiency both indicate that the TLL spin-labels are not that closely associated with the POPC membrane. For POPG LUV, the situation is different. We see a steeper distribution in the values of Φ and K_{SV}, indicating a closer and more distinct association of TLL with the POPG membrane. However, the values of K_{SV} are also more scattered in relation to the exposure factor, and the agreement between the two methods is reasonable.

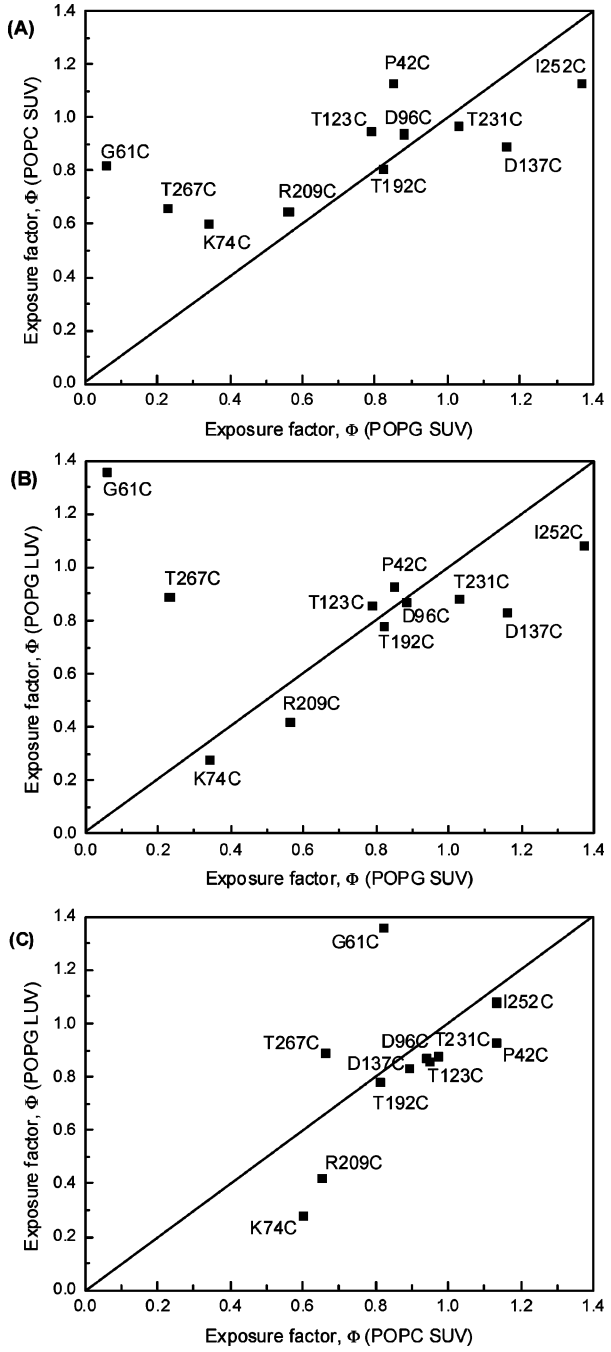

FIGURE 8: Comparison of values of the ESR exposure factor, Φ, for SL-TLLs bound to three different unilamellar phospholipid vesicles: (A) POPG SUV vs POPC SUV, (B) POPG SUV vs POPG LUV, and (C) POPC SUV vs POPG LUV. Values for POPG SUV were taken from ref *40*.

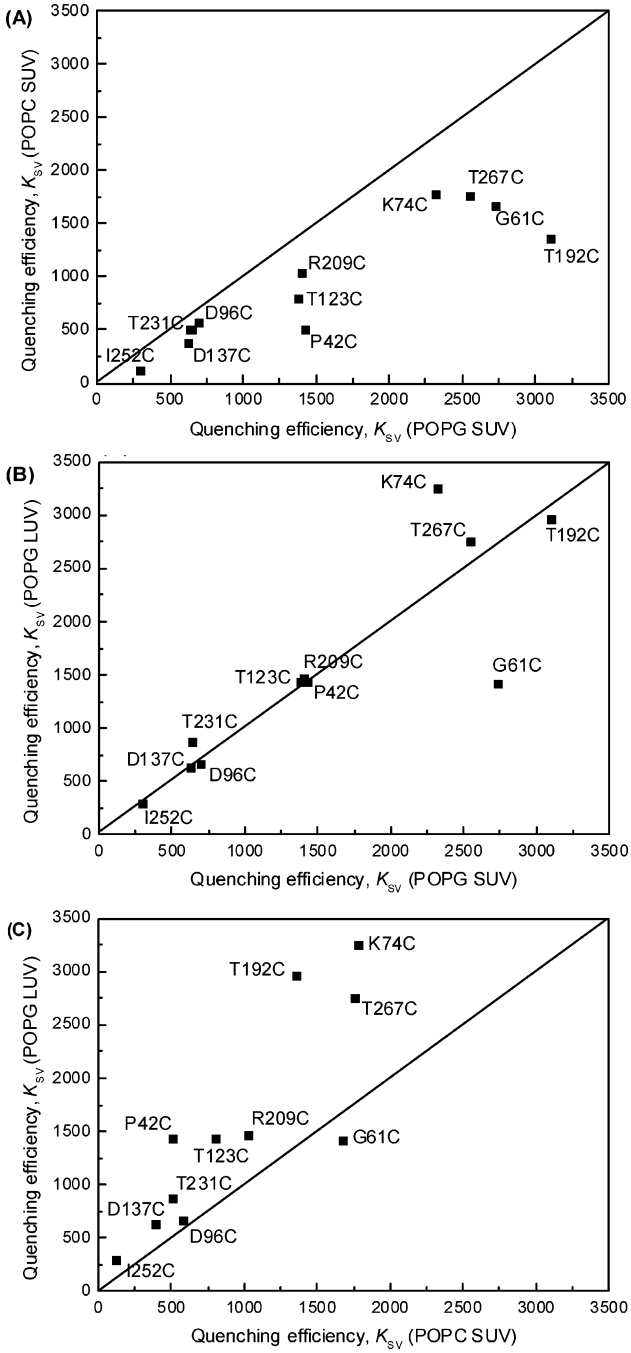

FIGURE 9: Comparison of values of the Stern−Volmer quenching constant, K_{SV}, for SL-TLLs bound to three different unilamellar phospholipid vesicles: (A) POPG SUV vs POPC SUV, (B) POPG SUV vs POPG LUV, and (C) POPC SUV vs POPG LUV. Values for POPG SUV were taken from ref *40*.

The orientation of TLL at the membrane surface of POPG SUV has previously been determined, using the same mutants and techniques as in the study presented here (*40*). TLL binds with high affinity to both small and large POPG vesicles, as well as to small POPC vesicles, but displays interfacial activation on only the small POPGs (*38*). The parameters Φ and K_{SV} obtained for the SL-TLLs are compared for the three vesicles in Figures 8 and 9, respectively. In Figure 8A−C, values of Φ are seen to be higher for the POPC SUV than for both of the POPG vesicles, signifying a higher level of Crox exposure all over. Markedly, the TLL contact residues found for POPG SUV in the productive (active) orientation (*40*), G61C-SL and T267C-SL, show a high degree of Crox exposure with both POPG LUV and POPC SUV. It can be concluded that the TLL orientations, inferred from the values of Φ, show the best convergence for POPG LUV and POPC SUV. This prevails even though the Crox gradient is different at the PC surface due to electrostatic effects. However, the distance between TLL and the membrane is greater with POPC SUV than with POPG LUV. In Figure 9A−C, it is evident that values of K_{SV} are lower for POPC SUV in all cases. This reinforces the notion that TLL binds farther from the PC surface than from both PG surfaces. There is quite good conformity for the K_{SV} values between the large and

small POPG vesicles. This suggests that TLL binds almost as closely to the two POPG vesicles. However, there are crucial discrepancies in some of the various contact residues, resulting in significant differences in the TLL orientation.

DISCUSSION

In this paper, the orientation of the fungal triglyceride lipase *T. lanuginosus* lipase (TLL) at the lipid−water interface of unilamellar phospholipid vesicles has been studied, employing site-directed spin-labeling (SDSL) in combination with ESR relaxation spectroscopy and fluorescence spectroscopy. Two types of vesicles have been used: large vesicles consisting of POPG carrying a negative surface charge and small vesicles consisting of POPC with a zwitterionic surface. In addition, the interactions of TLL with these vesicles have been compared to the results previously obtained with a third vesicle type, that of small POPG (*40*). Collectively, this has enabled assessment of the influence of vesicle properties, such as curvature and surface charge, on the detailed interfacial orientation of TLL.

Well-Defined Interface for Determination of TLL Orientation. Triglycerides are the natural substrates of triglyceride lipases, which, unlike the esterases, only display full activity at the lipid−water interface of an aggregated substrate (*12*). The physical state of the substrate is presumably a deciding factor for the difference in substrate specificity between lipases and esterases (*57*). Long-chain triglycerides or fatty acid esters are typically insoluble or poorly soluble in water. Thus, the lipase has to be able to recognize an insoluble or heavily aggregated substrate (*57*). A major and long-standing obstacle in assessing the binding and activity of triglyceride lipases is that the organizational state of triglycerides in aqueous solution is difficult to control (*13*). Triglycerides form droplets of uncontrolled polymorphism and adsorb onto available surfaces such as vessel walls or gas bubbles (*13*). This makes it nearly impossible to generate well-defined structures of known surface area. However, Berg et al. successfully utlilized phospholipid vesicles as a system of well-defined composition to which both lipase and substrate could bind, and react (*13*). Phospholipids are not substrates of triglyceride lipases, but serve faithfully as a diluent interface for TLL and for substrates partitioned at the surface, as well as for substrates included in the lipid bilayer during vesicle preparation (*13*, *38*). These considerations make phospholipid vesicles an excellent system for studying the lipid−water interfacial binding orientation of TLL, in molecular detail.

Spin-Label Interactions. In this study, the effect of the water-soluble paramagnetic spin-relaxation agent Crox on each protein-bound spin-label was measured by ESR spectroscopy for the SL-TLLs bound to the phospholipid vesicles with different surface charges and sizes. In this system, the exposure factor Φ (*40*, *41*) describes the interactions between Crox and the protein-bound nitroxide, taking place in the form of a bicollisional mechanism known as Heisenberg exchange, which increases the relaxation rates of the nitroxide (*58*). Thus, a reduction in Φ upon membrane binding can be comprehended in terms of a reduction in collision rates due to steric restrictions inflicted by the bilayer surface, and reduction of diffusion constants of the two partners (*58*).

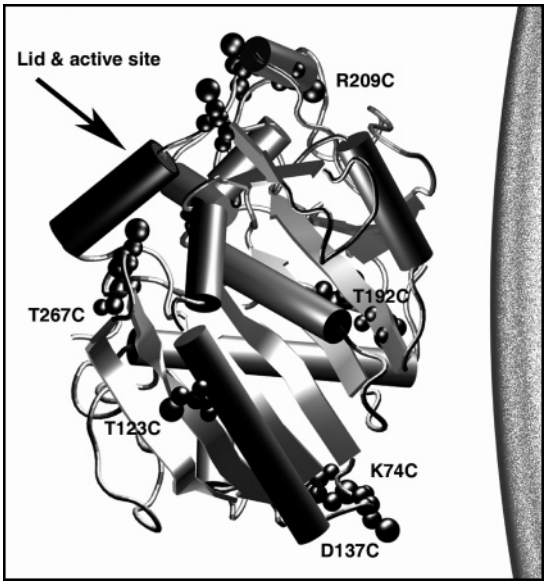

FIGURE 10: Suggested orientation of TLL at the interface of POPG LUV and POPC SUV. The representation of the vesicle surface is at the right. Distances from the membrane have not been precisely optimized herein. The distance from the interface is greater with POPC SUV. The same X-ray structure and software were used as in Figure 1.

Furthermore, electrostatic effects may be crucial in controlling the collisional kinetics for paramagnetic ions (*59*), which will be especially pronounced with a negatively charged vesicle surface. The local Crox concentration sensed by the nitroxide spin-label is a spatial average of the various conformations pertaining to the rapidly rotating nitroxide (*60*), where the length of the MTSL side chain is ∼6−7 Å. Determination of the low-amplitude parameter $\Delta c^{-1/2}$ (*48*), in the absence of vesicles, provides the effect of the local protein electrostatic potential on the concentration of Crox, granting a reference for the effect of Crox for each spin-labeled mutant (*61*).

Characteristics of TLL Spin-Label Interactions and Relation to Interfacial Orientation. The values of Φ obtained for the various spin-labeled TLLs bound to POPG LUV and to POPC SUV revealed that TLL preferentially adsorbs with a similar orientation on both vesicles, despite the fact that they carry different surface charges. The ESR data show that TLL binds with the concave backside of the protein facing the membrane surface, which is expected to correspond to the inactive orientation of TLL. This agrees well with the fluorescence and activity measurements presented by Cajal et al., showing weak activation on zwitterionic vesicles, as well as large POPG vesicles, when measured for the wild type, or tryptophan mutants of TLL (*38*). The contact surface defined vertically by the positions R209C-SL, T192C-SL, and K74C-SL found in our study, corresponding to the inactive orientation of TLL, is situated on the opposite side of the protein relative to the active-site catalytic Ser146. A suggestion for the preferred interfacial orientation of TLL on the POPG LUV and POPC SUV, based on the ESR and fluorescence data obtained in this study, is shown in Figure 10. The distances have not been optimized in this figure. Compared to the catalytically competent (*38*) orientation of TLL previously found on POPG SUV (*40*), the protein is rotated almost exactly 180° about its vertical axis in relation to the contact surface defined by G61C-SL, T267C-SL,

P42C-SL, and T123C-SL (*40*). Cajal et al. (*38*) hypothesized that the contact surface of TLL in the inactive form might coincide with the hydrophobic patch in the triangle defined by Trp89, Trp221, and Trp260. In this orientation, TLL would have to bind with T231C-SL, and especially I252C-SL, deeply embedded in the lipid membrane, which is clearly not the case as seen in the values of both Φ and K_{SV} for these mutants. Thus, this hypothesis is in complete disagreement with the inactive orientation found here, and does not match any of the orientations found for TLL on the various phospholipid vesicles (*40*).

Even though TLL adopts a similar orientation on both POPG LUV and POPC SUV, it is worth noting that the protein binds farther from the POPC surface, as indicated by the high and narrowly distributed values of Φ for POPC SUV. Interestingly, this difference in distance cannot be resolved in the values of K_d reported by Cajal et al., with (half the number of) 367 μM on POPG LUV and 308 μM on POPC SUV measured for the inactive TLL mutant Ser146Ala (*38*). Similar values were also obtained for the tryptophan mutants (*38*). However, in another study, Peters et al. (*62*) observed that TLL associated more weakly with PC liposomes than with PG liposomes. The authors hypothesized that the zwitterionic surface of the PC vesicles could result in a tight hydration shell around the headgroups, producing strong hydrogen bonding between water molecules and the charged nitrogen and phosphate groups, and that the hydration shell might affect the diffusion of TLL to the lipid surface (*62*). It is worth considering that for the zwitterionic surface of POPC vesicles, the concentration gradient of Crox at the lipid membrane compared to its bulk concentration should be different from that for the negatively charged POPG membrane, due to electrostatic effects. As discussed in the previous section, this could lead to apparent values of Φ that are too high, thus indicating that TLL is farther from the POPC surface than it really is. The influence of Crox concentration measured on the spin-labeled POPG and POPC vesicles demonstrated that Crox is in fact closer to the zwitterionic POPC surface at the headgroup level, but this does not conclusively show how the concentration varies with distance from the surface. The ESR relaxation data, which determine interactions of TLL spin-labels with the aqueous phase, were also complemented with the independent technique of fluorescence quenching. Since the nitroxide quenches the fluorescence of dansyl-labeled vesicles, this quantifies TLL spin-label interactions from the lipid side of the interface. Low values of the distance-dependent fluorescence quenching efficiency, K_{SV}, were obtained with dansyl-labeled POPC SUV, reinforcing the ESR data. Since the K_{SV} values describe the direct interaction between TLL spin-labels and the lipid fluorophore, significant artifacts in Φ due to Crox gradients can be ruled out. It can thus be concluded that TLL associates farther from the POPC surface than from that of POPG LUV. Generally, the values of Φ and K_{SV} showed good agreement for both vesicles, confirming the orientations found for TLL.

Sandwich Mode for TLL Bound to Phospholipid Vesicles. In our previous study of the active-mode orientation of TLL on POPG SUV, more than one exclusive orientation at the interface was indicated, although the active-mode orientation was largely predominant (*40*). Interestingly, fluorescence resonance energy transfer (FRET) experiments, employing vesicles labeled with a fluorescence donor and acceptor pair, confirmed that TLL was able to bind simultaneously (and reversibly) to two vesicles, bringing them into proximity (*40*). This suggested two binding modes for TLL on the phospholipid vesicles. The second of these modes corresponds well with the interfacial orientation found in this study. In fact, values of Φ obtained with POPG LUV and POPC SUV also indicate an average of at least two orientations, even if one of them is dominating. For this reason, we did not attempt to model the orientation of TLL (*40*, *41*) on the POPG LUV, since resolving more than one binding orientation would afford too many unknown parameters. In addition, electrostatically based modeling is not applicable for the neutral surface of POPC SUV. However, some indication of TLL spin-label distances to the membrane surface can in principle be inferred from the previously determined electrostatically based Crox gradient for POPG vesicles (*40*). This affords TLL nitroxide−membrane distances for K74C-SL and R209C-SL estimated to be 16 and 19 Å for POPG LUV and, with greater uncertainty, 23 and 24 Å for POPC SUV, respectively.

In the perspective of a lipase "sandwich mode", it is interesting to note that there are several cases in which proteins have been known or suggested to bind simultaneously to two vesicles, alone or mediated by another molecule. This was observed for bee venom PLA2 where mellitin, polymyxin B, or myelin basic protein allowed intervesicle exchange of lipid substrates (*63* and references therein). Also, human group IIA PLA2 (hGIIA) has been reported to form a supramolecular structure involving multiple LUV, and it was proposed that hGIIA could "roll over" to a nearby vesicle in the complex (*61*).

Protein−Membrane Distances. In the membrane docking of peripheral proteins, several driving forces are expected to be important. These include favorable long-range (10−15 Å) electrostatic interactions between charged residues on the protein surface and the membrane surface, hydrophobic interactions of surface-exposed apolar residues with partially exposed hydrocarbon chains in the membrane interior, and an entropically favored release of bound water from the membrane−protein interface upon binding (*57*, *64*). For TLL docked on the membrane of both small and large POPG vesicles, and small POPC vesicles, it is clear that there is only a limited contact surface and no deep penetration of protein residues into the membrane. Nevertheless, this is consistent with distances observed for several membrane-docked proteins. Sometimes, an optimal interaction between positively charged side chains and an anionic membrane surface is obtained when these charged residues lie several angstroms off the interface (*64*). As another aspect, for the nearly parallel docking orientation observed for the protein kinase Cα C2 domain, it was hypothesized that a lipid may be partially drawn up from the membrane into the protein (*65*). Indeed, lipid protrusions and membrane softness have been proposed to be important for enzymatic activity, where protrusions of single lipid molecules out of the bilayer plane are realized in the 10 ps time scale (*66*). These modes can be either collective or single-molecule-based (*66*). Direct evidence for an upward vertical displacement of lipid molecules has been obtained by ESR relaxation spectroscopy (*67*). Furthermore, in PLA2 the active site is ∼15 Å from the protein surface (*68*).

Driving Forces for Activation of TLL on Phospholipid Vesicles. It is interesting that TLL is activated 100-fold when bound to SUV POPG but not with LUV POPG, or with any POPC vesicles independently of vesicle size, despite the fact that TLL binds to all vesicles with similar dissociation constants (*38*). This indicates that the activation of the lipase is clearly separated from the adsorption step in the interfacial activation pathway. What, then, governs the activation and lid opening of the lipase when it has adsorbed to the lipid interface? The first discrete steps to the lid opening of TLL have been shown in X-ray structures to originate from Arg84 residing in the proximal hinge of the lid, acting as an "electrostatic sensor", and a molecular switch in conjunction with a nearby disulfide flip (*32*). This mechanism is in excellent agreement with the active-mode orientation of TLL found previously for SUV POPG (*40*), in which TLL binds with the arginine switch moiety in direct contact with the lipid membrane. In this study, TLL in the inactive mode was found to be oriented on POPG LUV and POPC SUV with the active site facing away from the membrane. Together, these results suggest that the orientation at the interface is a separate and crucial step for the enzymatic activation. A negative charge of the membrane surface seems to allow but not guarantee activation of TLL, and the same is true for a highly positive membrane curvature. Apparently, TLL is dependent on both attractive electrostatic forces and hydrophobic interactions, the latter acting to stabilize simultaneously as they facilitate substrate extraction (*38*).

Emerging Evidence of Unusual Activation Modes. There has been an increasing number of recent reports addressing the tendency of several microbial lipases, including TLL, to form bimolecular or larger aggregates (*69*, *70*). Lipases are distinguished by a dense cluster of hydrophobic side-chain residues, seen in the X-ray structures, which favors protein self-aggregation in aqueous solution (*23*). It is thought that the clusters are due to an increase in the number of valine, leucine, and isoleucine residues, which tend to collect around the active site of lipases (*57*). The fact that pig pancreatic IB PLA2 is able to form aggregates in the presence of alkyl sulfates, forming an $E^{\#}$ complex of half-micellar structure (*71*), has also emerged, and activation of TLL by various detergents also induced below the detergents' cmc has recently been reported (*17*). Extensive work has also been done to address the effect of monoolein self-assembly, morphology, and phase on TLL activity (see, for example, ref *72*). Perhaps most intriguing of all is the report of kinetically trapped, varying conformational states of different lipases, including TLL, achieved when employing a detergent in concentrations up to its cmc prior to rapid freeze-drying. The various trapped active forms of the lipases later permitted activity with triglycerides of increasing chain length, correlating to the treatment prior to trapping (*33*). Together with more recent X-ray data (*32*), this indicates evidence for a dynamic equilibrium and coexistence of closed and open forms and various intermediates thereof in aqueous solution, in which the closed form probably is largely favored for most lipases in the absence of an interface. All this points to an emerging view of more exquisite and complex mechanisms for enzyme activation, presumably with relevant biological significance for lipases. In this context, the different orientations of TLL at the phospholipid interfaces found in this study and previously (*40*), together with the TLL sandwich mode, conform very well.

REFERENCES

1. Winkler, F. K., D'Arcy, A., and Hunziker, W. (1990) Structure of Human Pancreatic Lipase, *Nature 343*, 771−774.
2. Mukherjee, K. D., and Hills, M. J. (1994) Lipases from plants, in *Lipases: Their Structure, Biochemistry and Application* (Woolley, P., and Petersen, S. B., Eds.) pp 49−75, Cambridge University Press, Cambridge, U.K.
3. Jaeger, K. E., Ransac, S., Dijkstra, B. W., Colson, C., Vanheuvel, M., and Misset, O. (1994) Bacterial Lipases, *FEMS Microbiol. Rev. 15*, 29−63.
4. Sidebottom, C. M., Charton, E., Dunn, P. P. J., Mycock, G., Davies, C., Sutton, J. L., Macrae, A. R., and Slabas, A. R. (1991) *Geotrichum candidum* Produces Several Lipases with Markedly Different Substrate Specificities, *Eur. J. Biochem. 202*, 485−491.
5. Iwai, M., and Tsujisaka, Y. (1984) Fungal lipase, in *Lipases* (Borgström, B., and Brockman, H. L., Eds.) pp 443−469, Elsevier, Amsterdam.
6. Peters, G. H., and Bywater, R. P. (2001) Influence of a lipid interface on protein dynamics in a fungal lipase, *Biophys. J. 81*, 3052−3065.
7. Beisson, F., Tiss, A., Rivière, C., and Verger, R. (2000) Methods for lipase detection and assay: A critical review, *Eur. J. Lipid Sci. Technol. 102*, 133−153.
8. Schmid, R. D., and Verger, R. (1998) Lipases: Interfacial enzymes with attractive applications, *Angew. Chem., Int. Ed. 37*, 1609−1633.
9. Faber, K. (1992) *Biotransformations in Organic Chemistry*, Springer-Verlag, Berlin.
10. Holmquist, M. (2000) α/β-Hydrolase Fold Enzymes: Structures, Functions and Mechanisms, *Curr. Protein Pept. Sci. 1*, 209−235.
11. Ollis, D. L., Cheah, E., Cygler, M., Dijkstra, B., Frolow, F., Franken, S. M., Harel, M., Remington, S. J., Silman, I., Schrag, J., Sussman, J. L., Verschueren, K. H. G., and Goldman, A. (1992) The α/β-Hydrolase Fold, *Protein Eng. 5*, 197−211.
12. Sarda, L., and Desnuelle, P. (1958) Actions of pancreatic lipase on esters in emulsions, *Biochim. Biophys. Acta 30*, 513−521.
13. Berg, O. G., Cajal, Y., Butterfoss, G. L., Grey, R. L., Alsina, M. A., Yu, B. Z., and Jain, M. K. (1998) Interfacial activation of triglyceride lipase from *Thermomyces (Humicola) lanuginosa*: Kinetic parameters and a basis for control of the lid, *Biochemistry 37*, 6615−6627.
14. Yu, B. Z., Berg, O. G., and Jain, M. K. (1999) Hydrolysis of monodisperse phosphatidylcholines by phospholipase A2 occurs on vessel walls and air bubbles, *Biochemistry 38*, 10449−10456.
15. Jutila, A., Zhu, K., Patkar, S. A., Vind, J., Svendsen, A., and Kinnunen, P. K. J. (2000) Detergent-induced conformational changes of *Humicola lanuginosa* lipase studied by fluorescence spectroscopy, *Biophys. J. 78*, 1634−1642.
16. Zhu, K., Jutila, A., Tuominen, E. K. J., and Kinnunen, P. K. J. (2001) Effects of *i*-propanol on the structural dynamics of *Thermomyces lanuginosa* lipase revealed by tryptophan fluorescence, *Protein Sci. 10*, 339−351.
17. Mogensen, J. E., Sehgal, P., and Otzen, D. E. (2005) Activation, inhibition, and destabilization of *Thermomyces lanuginosus* lipase by detergents, *Biochemistry 44*, 1719−1730.
18. Brady, L., Brzozowski, A. M., Derewenda, Z. S., Dodson, E., Dodson, G., Tolley, S., Turkenburg, J. P., Christiansen, L., Huge-Jensen, B., Norskov, L., Thim, L., and Menge, U. (1990) A Serine Protease Triad Forms the Catalytic Center of a Triacylglycerol Lipase, *Nature 343*, 767−770.
19. Schrag, J. D., Li, Y., Wu, S., and Cygler, M. (1991) Ser-His-Glu Triad Forms the Catalytic Site of the Lipase From *Geotrichum candidum*, *Nature 351*, 761−764.
20. Grochulski, P., Li, Y. G., Schrag, J. D., Bouthillier, F., Smith, P., Harrison, D., Rubin, B., and Cygler, M. (1993) Insights Into Interfacial Activation From an Open Structure of *Candida rugosa* Lipase, *J. Biol. Chem. 268*, 12843−12847.
21. Noble, M. E. M., Cleasby, A., Johnson, L. N., Egmond, M. R., and Frenken, L. G. J. (1993) The Crystal-Structure of Triacylglycerol Lipase From *Pseudomonas glumae* Reveals a Partially Redundant Catalytic Aspartate, *FEBS Lett. 331*, 123−128.
22. Lawson, D. M., Brzozowski, A. M., Dodson, G. G., Hubbard, R. E., Huge-Jensen, B., Boel, E., and Derewenda, Z. S. (1994) in

Lipases: Their biochemistry, structure and application (Petersen, S., Ed.) pp 77−94, Cambridge University Press, Cambridge, U.K.
23. Brzozowski, A. M., Derewenda, U., Derewenda, Z. S., Dodson, G. G., Lawson, D. M., Turkenburg, J. P., Björkling, F., Huge-Jensen, B., Patkar, S. A., and Thim, L. (1991) A Model For Interfacial Activation in Lipases from the Structure of a Fungal Lipase-Inhibitor Complex, *Nature 351*, 491−494.
24. van Tilbeurgh, H., Egloff, M. P., Martinez, C., Rugani, N., Verger, R., and Cambillau, C. (1993) Interfacial Activation of the Lipase Procolipase Complex By Mixed Micelles Revealed By X-ray Crystallography, *Nature 362*, 814−820.
25. Grochulski, P., Bouthillier, F., Kazlauskas, R. J., Serreqi, A. N., Schrag, J. D., Ziomek, E., and Cygler, M. (1994) Analogs of Reaction Intermediates Identify a Unique Substrate-Binding Site in *Candida rugosa* Lipase, *Biochemistry 33*, 3494−3500.
26. Lawson, D. M., Brzozowski, A. M., Rety, S., Verma, C., and Dodson, G. G. (1994) Probing the Nature of Substrate-Binding in *Humicola lanuginosa* Lipase Through X-ray Crystallography and Intuitive Modeling, *Protein Eng. 7*, 543−550.
27. Hermoso, J., Pignol, D., Penel, S., Roth, M., Chapus, C., and Fontecilla-Camps, J. C. (1997) Neutron crystallographic evidence of lipase-colipase complex activation by a micelle, *EMBO J. 16*, 5531−5536.
28. Derewenda, U., Brzozowski, A. M., Lawson, D. M., and Derewenda, Z. S. (1992) Catalysis At the Interface: The Anatomy of a Conformational Change in a Triglyceride Lipase, *Biochemistry 31*, 1532−1541.
29. Grochulski, P., Li, Y., Schrag, J. D., and Cygler, M. (1994) 2 Conformational States of *Candida rugosa* Lipase, *Protein Sci. 3*, 82−91.
30. Peters, G. H., Toxvaerd, S., Olsen, O. H., and Svendsen, A. (1997) Computational studies of the activation of lipases and the effect of a hydrophobic environment, *Protein Eng. 10*, 137−147.
31. Derewenda, Z. S. (1995) A Twist in the Tale of Lipolytic Enzymes, *Nat. Struct. Biol. 2*, 347−349.
32. Brzozowski, A. M., Savage, H., Verma, C. S., Turkenburg, J. P., Lawson, D. M., Svendsen, A., and Patkar, S. (2000) Structural origins of the interfacial activation in *Thermomyces (Humicola) lanuginosa* lipase, *Biochemistry 39*, 15071−15082.
33. González-Navarro, H., Bañó, M. C., and Abad, C. (2001) The closed/open model for lipase activation. Addressing intermediate active forms of fungal enzymes by trapping of conformers in water-restricted environments, *Biochemistry 40*, 3174−3183.
34. Martinelle, M., Holmquist, M., and Hult, K. (1995) On the Interfacial Activation of *Candida antarctica* Lipase A and Lipase B As Compared With *Humicola lanuginosa* Lipase, *Biochim. Biophys. Acta 1258*, 272−276.
35. Svendsen, A., Clausen, I. G., Patkar, S. A., Borch, K., and Thellersen, M. (1997) Protein engineering of microbial lipases of industrial interest, *Methods Enzymol. 284*, 317−340.
36. Holmquist, M., Martinelle, M., Clausen, I. G., Patkar, S., Svendsen, A., and Hult, K. (1994) Trp89 in the Lid of *Humicola lanuginosa* Lipase Is Important For Efficient Hydrolysis of Tributyrin, *Lipids 29*, 599−603.
37. Petersen, M. T. N., Fojan, P., and Petersen, S. B. (2001) How do lipases and esterases work: The electrostatic contribution, *J. Biotechnol. 85*, 115−147.
38. Cajal, Y., Svendsen, A., Girona, V., Patkar, S. A., and Alsina, M. A. (2000) Interfacial control of lid opening in *Thermomyces lanuginosa* lipase, *Biochemistry 39*, 413−423.
39. Hubbell, W. L., Cafiso, D. S., and Altenbach, C. (2000) Identifying conformational changes with site-directed spin labeling, *Nat. Struct. Biol. 7*, 735−739.
40. Hedin, E. M. K., Høyrup, P., Patkar, S. A., Vind, J., Svendsen, A., Fransson, L., and Hult, K. (2002) Interfacial orientation of *Thermomyces lanuginosa* lipase on phospholipid vesicles investigated by electron spin resonance relaxation spectroscopy, *Biochemistry 41*, 14185−14196.
41. Lin, Y., Nielsen, R., Murray, D., Hubbell, W. L., Mailer, C., Robinson, B. H., and Gelb, M. H. (1998) Docking phospholipase A2 on membranes using electrostatic potential-modulated spin relaxation magnetic resonance, *Science 279*, 1925−1929.
42. Berg, S. P., and Nesbitt, D. M. (1979) Chromium Oxalate: New Spin Label Broadening Agent for Use with Thylakoids, *Biochim. Biophys. Acta 548*, 608−615.
43. Bailar, J. C., and Jones, E. M. (1939) Trioxalato salts, *Inorg. Synth. 1*, 35−38.
44. Hedin, E. M. K., Patkar, S. A., Vind, J., Svendsen, A., Hult, K., and Berglund, P. (2002) Selective reduction and chemical modification of oxidized lipase cysteine mutants, *Can. J. Chem. 80*, 529−539.
45. Pace, C. N., Vajdos, F., Fee, L., Grimsley, G., and Gray, T. (1995) How to Measure and Predict the Molar Absorption-Coefficient of a Protein, *Protein Sci. 4*, 2411−2423.
46. Abel, E., Maguire, G. E. M., Murillo, O., Suzuki, I., De Wall, S. L., and Gokel, G. W. (1999) Hydraphile channels: Structural and fluorescent probes of position and function in a phospholipid bilayer, *J. Am. Chem. Soc. 121*, 9043−9052.
47. Poole, C. P., Jr. (1967) *Electron Spin Resonance: A Comprehensive Treatise on Experimental Techniques*, Interscience Publishers, New York.
48. Hedin, E. M. K., Hult, K., Mouritsen, O. G., and Høyrup, P. (2004) Low microwave-amplitude ESR spectroscopy: Measuring spin-relaxation interactions of moderately immobilized spin labels in proteins, *J. Biochem. Biophys. Methods 60*, 117−138.
49. Haas, D. A., Mailer, C., and Robinson, B. H. (1993) Using Nitroxide Spin Labels: How to Obtain T_{1e} From Continuous Wave Electron Paramagnetic Resonance Spectra at All Rotational Rates, *Biophys. J. 64*, 594−604.
50. Pake, G. E., and Tuttle, T. R., Jr. (1959) Anomalous loss of resolution of paramagnetic resonance hyperfine structure in liquids, *Phys. Rev. 3*, 423−425.
51. Altenbach, C., Flitsch, S. L., Khorana, H. G., and Hubbell, W. L. (1989) Structural Studies on Transmembrane Proteins 2. Spin Labeling of Bacteriorhodopsin Mutants at Unique Cysteines, *Biochemistry 28*, 7806−7812.
52. Hubbell, W. L., Gross, A., Langen, R., and Lietzow, M. A. (1998) Recent advances in site-directed spin labeling of proteins, *Curr. Opin. Struct. Biol. 8*, 649−656.
53. Mchaourab, H. S., Lietzow, M. A., Hideg, K., and Hubbell, W. L. (1996) Motion of spin-labeled side chains in T4 lysozyme, correlation with protein structure and dynamics, *Biochemistry 35*, 7692−7704.
54. Columbus, L., and Hubbell, W. L. (2004) Mapping backbone dynamics in solution with site-directed spin labeling: GCN4-58 bZip free and bound to DNA, *Biochemistry 43*, 7273−7287.
55. Zhang, Z. X., Melia, T. J., He, F., Yuan, C., McGough, A., Schmid, M. F., and Wensel, T. G. (2004) How a G protein binds a membrane, *J. Biol. Chem. 279*, 33937−33945.
56. Gilmanshin, R., Creutz, C. E., and Tamm, L. K. (1994) Annexin IV Reduces the Rate of Lateral Lipid Diffusion and Changes the Fluid-Phase Structure of the Lipid Bilayer When It Binds to Negatively Charged Membranes in the Presence of Calcium, *Biochemistry 33*, 8225−8232.
57. Fojan, P., Jonson, P. H., Petersen, M. T. N., and Petersen, S. B. (2000) What distinguishes an esterase from a lipase: A novel structural approach, *Biochimie 82*, 1033−1041.
58. Altenbach, C., Froncisz, W., Hyde, J. S., and Hubbell, W. L. (1989) Conformation of Spin-Labeled Melittin At Membrane Surfaces Investigated By Pulse Saturation Recovery and Continuous Wave Power Saturation Electron-Paramagnetic Resonance, *Biophys. J. 56*, 1183−1191.
59. Marsh, D., Páli, T., and Horváth, L. I. (1998) Progressive Saturation and Saturation Transfer EPR for Measuring Exchange Processes and Proximity Relations in Membranes, in *Biological Magnetic Resonance, Spin Labeling: The Next Millennium* (Berliner, L. J., Ed.) pp 23−82, Plenum Press, New York.
60. Addona, G. H., Andrews, S. H., and Cafiso, D. S. (1997) Estimating the electrostatic potential at the acetylcholine receptor agonist site using power saturation EPR, *Biochim. Biophys. Acta 1329*, 74−84.
61. Canaan, S., Nielsen, R., Ghomashchi, F., Robinson, B. H., and Gelb, M. H. (2002) Unusual mode of binding of human group IIA secreted phospholipase A2 to anionic interfaces as studied by continuous wave and time domain electron paramagnetic resonance spectroscopy, *J. Biol. Chem. 277*, 30984−30990.
62. Peters, G. H., Svendsen, A., Langberg, H., Vind, J., Patkar, S. A., and Kinnunen, P. K. J. (2002) Glycosylation of *Thermomyces lanuginosa* lipase enhances surface binding towards phospholipids, but does not significantly influence the catalytic activity, *Colloids Surf., B 26*, 125−134.
63. Cajal, Y., and Jain, M. K. (1997) Synergism between mellitin and phospholipase A2 from bee venom: Apparent activation by intervesicle exchange of phospholipids, *Biochemistry 36*, 3882−3893.
64. Frazier, A. A., Wisner, M. A., Malmberg, N. J., Victor, K. G., Fanucci, G. E., Nalefski, E. A., Falke, J. J., and Cafiso, D. S.

(2002) Membrane orientation and position of the C2 domain from cPLA2 by site-directed spin labeling, *Biochemistry 41*, 6282−6292.
65. Kohout, S. C., Corbalán-García, S., Gómez-Fernández, J. C., and Falke, J. J. (2003) C2 domain of protein kinase Cα: Elucidation of the membrane docking surface by site-directed fluorescence and spin labeling, *Biochemistry 42*, 1254−1265.
66. Høyrup, P., Callisen, T. H., Jensen, M. O., Halperin, A., and Mouritsen, O. G. (2004) Lipid protrusions, membrane softness, and enzymatic activity, *Phys. Chem. Chem. Phys. 6*, 1608−1615.
67. Arora, A., and Marsh, D. (1998) Protein-induced vertical lipid dislocation in a model membrane system: Spin-label relaxation studies on avidin−biotinylphosphatidylethanolamine interactions, *Biophys. J. 75*, 2915−2922.
68. Scott, D. L., White, S. P., Otwinowski, Z., Yuan, W., Gelb, M. H., and Sigler, P. B. (1990) Interfacial Catalysis: The Mechanism of Phospholipase A2, *Science 250*, 1541−1546.
69. Fernández-Lorente, G., Palomo, J. M., Fuentes, M., Mateo, C., Guisán, J. M., and Fernández-Lafuente, R. (2003) Self-assembly of *Pseudomonas fluorescens* lipase into bimolecular aggregates dramatically affects functional properties, *Biotechnol. Bioeng. 82*, 232−237.
70. Palomo, J. M., Fuentes, M., Fernández-Lorente, G., Mateo, C., Guisan, J. M., and Fernández-Lafuente, R. (2003) General trend of lipase to self-assemble giving bimolecular aggregates greatly modifies the enzyme functionality, *Biomacromolecules 4*, 1−6.
71. Yu, B. Z., Apitz-Castro, R., Tsai, M. D., and Jain, M. K. (2003) Interaction of monodisperse anionic amphiphiles with the i-face of secreted phospholipase A2, *Biochemistry 42*, 6293−6301.
72. Borné, J., Nylander, T., and Khan, A. (2002) Effect of lipase on monoolein-based cubic phase dispersion (cubosomes) and vesicles, *J. Phys. Chem. B 106*, 10492−10500.
73. Humphrey, W., Dalke, A., and Schulten, K. (1996) VMD: Visual Molecular Dynamics, *J. Mol. Graphics 14.1*, 33−38.

BI051478O